Journal of Power Sources 269 (2014) 418–423

Contents lists available at ScienceDirect

Journal of Power Sources

journal homepage: www.elsevier.com/locate/jpowsour

Effects of polymeric binders on electrochemical performances of spinel lithium manganese oxide cathodes in lithium ion batteries

Sangmin Lee [a, 1], Eun-Young Kim [b, 1], Hochun Lee [b, **], Eun-Suok Oh [a, *]

[a] School of Chemical Engineering, University of Ulsan, 93 Daehak-ro, Ulsan 680-749, Republic of Korea
[b] Department of Energy Systems Engineering, Daegu Gyeongbuk Institute of Science and Technology (DGIST), Daegu 711-873, Republic of Korea

HIGHLIGHTS

- Four types of polymers are adopted as binders for spinel LMO electrodes.
- Binder film on the surface of LMO plays a role of passivation layer for Mn dissolution.
- PAN-LMO electrodes exhibit superior rate capability, thermal stability, and low Mn dissolution.
- PAN is revealed to be an outstanding binder for LMO, compared to PVdF and other binders.

ARTICLE INFO

Article history:
Received 20 May 2014
Received in revised form
11 June 2014
Accepted 13 June 2014
Available online 9 July 2014

Keywords:
Spinel lithium manganese oxide
Manganese dissolution
Binder
Polyacrylonitrile

ABSTRACT

Effects of polymeric binders on both the dissolution of manganese (Mn) and electrochemical properties of spinel $LiMn_2O_4$ (LMO) electrodes are investigated in detail. Three promising polymers, polyvinyl alcohol (PVA), polyacrylic acid (PAA), and polyacrylonitrile (PAN) are chosen as binders for the LMO electrodes and compared to currently popular polyvinylidene fluoride (PVdF). For LMO electrodes fabricated with the selected binders, physicochemical properties including surface coverage, adhesion strength, and electrolyte uptake are examined. Also, electrochemical performance factors such as Mn dissolution behavior, rate capability, cycle performance, and thermal stability are investigated. PAN is revealed to be an outstanding binder for LMO electrodes based on its excellent rate capability, superior cycle performance, and high thermal stability when compared to the other three binders. This can be ascribed to an appropriate amount of electrolyte uptake and low impedance of the PAN despite the relatively large surface coverage of the LMO that leads to lower Mn dissolution.

1. Introduction

Due to its superior electrochemical performance, low cost, and environmental inertness, spinel $LiMn_2O_4$ (LMO) is considered a promising cathode material for lithium ion batteries (LIBs), especially for large scale applications such as electric vehicles and energy storage systems [1,2] The poor thermal stability of LMO, however, mainly due to manganese (Mn) dissolution at elevated temperatures, has hampered its progress in new applications [3–12]. It is generally known that Mn dissolution is associated with a disproportionation reaction which liberates soluble Mn^{2+} into electrolyte:

$$Mn^{3+}(\text{electrode}) \rightarrow Mn^{4+}(\text{electrode}) + Mn^{2+}(\text{electrolyte})$$ [2–9].

Then, the dissolved Mn^{2+} moves to the anode and exacerbates degradation of the anode/electrolyte interface, which is revealed to be a key failure mechanism of LMO-based LIBs at elevated temperature [9–12].

So far, extensive studies have been devoted to suppress Mn dissolution, and thus to improve long-term stability of LMO. Most of the attempts have been made to modify the LMO itself in order to enhance its structural stability, [13–15] or to develop functional electrolyte additives to stifle Mn dissolution from LMO or subsequent Mn deposition on the anode [16–21]. In contrast, minimal attention has been paid to the inactive components of LIB electrodes: polymeric binders and conductive carbons [22–25].

In particular, the crucial role of polymeric binders in LIB performance has been recently highlighted [26–31]. The polymeric binder provides integrity within the LIB composite electrode by promoting adhesion among the particles of active materials and between active materials and the current collector. Currently, only

* Corresponding author. Tel.: +82 52 259 2783; fax: +82 52 259 1689.
** Corresponding author. Tel.: +82 53 785 6411; fax: +82 53 785 6409.
E-mail addresses: dukelee@dgist.ac.kr (H. Lee), esoh1@ulsan.ac.kr (E.-S. Oh).
[1] Equally contributed to this work.

http://dx.doi.org/10.1016/j.jpowsour.2014.06.167
0378-7753/

two types of binder systems are being widely adopted in the LIB industry: polyvinylidene fluoride (PVdF) dissolved in N-methyl-2-pyrrolidone (NMP) and carboxymethyl cellulose (CMC) combined with styrene-butadiene rubber (SBR) emulsified in water [32–36]. Besides these polymers, a variety of polymers have been recently investigated as potential binders for LIB electrodes such as polyvinyl alcohol (PVA), polyacrylic acid (PAA), polyacrylonitrile (PAN), polyimide (PI), and polysaccharide [28–31,37,38]. Such binders gained attention not only due to their novel binding modes, but also due to their additional properties such as artificial surface passivation for irreversible reactions and mechanical buffer effect for volume change accompanying LIB operation.

PVA binder containing numerous hydroxyl groups in its polymer chain makes strong hydrogen bonds with active materials and the current collector, which is favorable for decreasing volumetric change and preventing excessive electrolyte uptake [30]. PAA binder, the most frequently studied polymer in recent years [28,37,39–42], has been reported to serve as an artificial SEI layer on the surface of active materials. In addition, PAA binder was claimed to be able to maintain the electric network of the SiO anode during cycles, resulting in improved cyclic performance [29]. PAN binder containing a strongly polar nitrile group was also demonstrated to be an efficient binder for various LIB anodes such as graphite, silicon/graphite and lithium titanium oxide [31].

Such studies on binders have mainly focused on LIB anodes. Much less attention has been paid to the cathode side. Although some recent reports claimed that cellulose-based polymers and ionomer binders improved cyclic performance and rate capability of LMO cathodes due to their better structural stability, stronger binding ability and smaller resistance [22,23,43,44], systematic comparison between various binders regarding electrochemical properties of LMO electrodes is still absent. In this study, three promising polymers, PVA, PAA, and PAN as binders for LMO electrodes are compared with the currently most popular PVdF binder. For LMO electrodes fabricated with the selected binders, fundamental properties including surface coverage, adhesion strength, and electrolyte uptake were examined. Then, the Mn dissolution behavior and electrochemical performances of the LMO electrodes were investigated.

2. Experimental

Three commercially available polymers were used as binders; PVdF (KF9130, Kureha), PAN (Mw = 150,000, Aldrich), and PAA (Mw = 3,000,000, Aldrich). Meanwhile high molecular weight PVA with 94% degree of saponification (the number of hydroxyl groups in 100 vinyl units of PVA), which showed excellent binding properties, was synthesized using the procedure described in our previous study [30]. Their chemical structures are shown in Fig. 1.

Cathode slurry was prepared by combining 92 wt.% LMO (commercial grade, Posco ESM) with 3 wt.% Super-p as a conductive material and 5 wt.% binder in n-methyl-2-pyrrolidone solvent. Dimethyl sulfoxide was used as a solvent for PVA binder. The slurry was mixed by a ball mill (Pulverisette 7, Fritsch) with two 10 mm zirconia beads in a 45 ml zirconia jar. It was programmed to repeatedly rotate in both directions 8 times with the rotational speed of 380 rpm. Each rotation was performed for 8 min so that total mixing time was approximately 1 h. The resultant was coated on aluminum foil, and finally dried in a convection oven at 130 °C for 20 min followed by vacuum drying at 80 °C overnight. The loading of the composite electrodes was 10.8 mg ± 0.3 mg cm^{-2}.

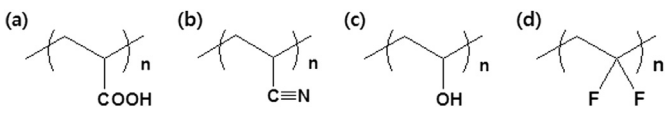

Fig. 1. Chemical structures of the polymers used as binders: (a) PAA, (b) PAN, (c) PVA, and (d) PVdF.

The graphite electrode was fabricated by coating a mixture of natural graphite (DAG-87, Sodiff), 1.5 wt.% SBR and 1 wt.% CMC binder on copper foil (10 μm). As an electrolyte, 1 M $LiPF_6$ in ethylene carbonate (EC) and ethyl methyl carbonate (EMC) (3/7 v/v, LG Chem) was used throughout this study.

To examine the Mn dissolution behavior, one piece of the LMO electrode (14 mm diameter) was stored in a PTFE bottle with 4 ml of the electrolyte at 60 °C for 7 days. To avoid possible errors due to leakage during storage, the weights of the closed PTFE bottles before and after the storage were checked, and the subsequent analysis was performed only when the weight loss was negligible. To determine the dissolved Mn^{2+} concentration, 0.5 ml of electrolyte was sampled and diluted with distilled water by a factor of 10, and then the diluted solution was analyzed by atomic absorption spectroscopy (AA-7000, Shimadzu). Simultaneously, water and HF contents were analyzed by Karl Fisher (831 KF coulometer, Metrohm) and acid-base titration methods (848 Titrino plus, Metrohm), respectively.

For electrochemical tests, 2016 or 2032-type coin cells employing the LMO cathode containing each binder and a Li-metal or graphite anode with a polyethylene separator (20 μm, Tonen) were assembled in an Ar-filled glove box. All the cells were cycled initially at 25 °C over a 3.0–4.3 V range three times with 0.2C (1C = 93.4 mAh g^{-1}) constant current (CC) charging followed by 4.3 V constant voltage (CV) charging and 0.2C CC discharging to complete the formation process. Rate capability testing was carried out for LMO/Li cells with 0.2C CC/CV charging and various CC discharging over 3.0–4.3 V at 25 °C. Cycle tests were performed for LMO/graphite cells with 0.5C CC/CV and 0.5C CC over 3.0–4.3 V, both at 25 °C and 60 °C. Electrochemical impedance spectra (EIS) were obtained for fully discharged LMO/Li cells before and after 24 h storage at 60 °C. All the measurements were performed at room temperature using a potentiostat (Biologic VSP) with a built-in EIS analyzer. The frequency range was 100 kHz to 10 mHz, the ac amplitude was 5 mV, and the dc bias voltage was 3.8 V.

The adhesion strength and surface elements of the LMO electrodes were determined at 180 peel strength measured using a texture analyzer (TA-PLUS, Lloyd), and by X-ray photoelectron spectroscopy (ESCALAB 250, Thermo Fisher Sci.) using an Al Ka X-ray source scanning from 0 to 1200 eV, respectively. The electrolyte uptake of the binder films was measured in order to compare the electrolyte wettability of the binder. The pristine binder films (approximately 20 μm) were soaked in electrolyte for 48 h and the change in weight before and after soaking was measured as the amount of electrolyte uptake.

3. Results and discussions

3.1. Effects of binders on Mn dissolution of LMO electrodes

First of all, the effect of polymeric binder on Mn dissolution was investigated by measuring the amount of Mn dissolved from the LMO electrodes prepared with the four types of binders (hereafter called PAA-, PAN-, PVA-, PVdF-LMO, respectively). The electrodes were stored in an electrolyte solution at 60 °C for 7 days and the dissolved amounts of Mn^{2+} including H_2O and HF in the electrolyte were measured and listed in Table 1.

It is noted that PAN- and PVA-LMO exhibit relatively lower amounts of Mn dissolution than PAA- and PVdF-LMO. The amount of Mn dissolution is in the following order: PVA < PAN < PAA ≤ PVdF. While the variation in the water content is negligible, the HF

Table 1
The amounts of H_2O, HF, and Mn^{2+} dissolved from LMO electrodes fabricated with four different binders. The electrodes were stored with electrolyte at 60 °C for 7 days.

Binder	[H_2O] (ppm)	[HF] (ppm)	[Mn^{2+}] (ppm)
PAA	9.8	94.79	3.43
PAN	8.5	39.57	1.14
PVA	6.3	211.20	0.72
PVdF	7.5	112.00	3.58

concentration is in the following order: PAN < PAA ≤ PVdF < PVA. Except PVA, Mn dissolution is found to be proportional to HF content for the other three binders, which is consistent with HF-catalyzed Mn dissolution behavior [6–9]. Therefore, the suppressed Mn dissolution in PAN-LMO can partly be ascribed to the low HF content. The minimum Mn dissolution in PVA-LMO, however, is in contrast to its highest HF content. The high HF content in PVA-LMO is supposed to be due to its large amount of water absorption, probably due to the number of hydroxyl groups in the PVA backbone (Fig. 1c) [45]. The water held within the PVA-LMO seems to be dissolved out into the electrolyte during the 60 °C long-term storage and converted to HF through a hydrolysis reaction with $LiPF_6$ [46–48].

Besides the HF effect, a recent study highlighted the important role of chemical interaction between the functional groups in the binder and Mn^{2+} ions in preventing Mn dissolution [22]. It was claimed that numerous carboxyl and hydroxyl groups in the alginate binder strongly interacted with the Mn^{2+} ions by the egg-box model [49–51] and trapped them within the polymeric chain. Consequently, the alginate binder was more effective in reducing Mn dissolution than the conventional PVdF binder. Similarly, PVA and PAN binders containing polar hydroxyl and nitrile groups, respectively, may hamper Mn^{2+} ion transport through them. Unfortunately, the assumption fails to explain why PAA-LMO exhibits relatively high Mn dissolution, although PAA also consists of highly polar carboxyl groups that can form strong electrostatic interactions with Mn^{2+} ions.

In brief, these results indicate that other aspects besides HF content and chemical interaction with Mn^{2+} ions should be also considered to fully understand the binder effects on Mn dissolution behavior of LMO electrodes.

3.2. Binder coverage on LMO surface

In general, polymer binders are inhomogeneously distributed on the surface of active materials due to inhomogeneous existence of polar dangle bonds, which can attract polar groups of the binders. Yoo et al. [52] indicated that approximately 50% of PVdF was placed at the edge of graphite particles. The remaining parts of binder covered some portion of the surface of the active materials. It was also claimed that a maximum of 40% of the graphite surface was discretely covered by PVdF binder, whereas the rest of the surface was directly exposed to electrolyte. Similarly, our previous XPS results [30,31] indicated that the surface coverage by polymer binders was in the range of 18–50% depending on the type of binders and active materials. The binders that form strong interactions with active materials such as PVA and PAN are expected to cover a larger portion of the surfaces of the active materials than conventional PVdF did. Such a difference in the surface coverage by binders may be a crucial factor for the dissolution of Mn^{2+} ions because the ionic conductivity of the polymeric binder film is much lower (ca. 10^{-8} S cm^{-1} [28,53]) than that in liquid electrolytes (ca. 10^{-2}–10^{-3} S cm^{-1} [54–57]). Thus, from the viewpoint of ionic conduction, the binder film can serve as a passivation layer for the movement of Mn^{2+} ions from the LMO surface to the electrolyte.

In order to investigate the coverage of the LMO surface by the binder, the XPS measurement of the pristine LMO electrodes was performed, and the Mn 2p spectra are displayed in Fig. 2. The peak intensities are quantitatively proportional to bare Mn atoms that are not covered by the binders, and directly exposed to the electrolyte solution. Compared to the PAA- or PVdF-LMO electrodes, the PVA- and PAN-LMO electrodes exhibit much reduced peak intensities. It seems that PAN and PVA interacting strongly with LMO active materials cover a broader surface of the LMO compared with the PAA and PVdF binder. In particular, strong hydrogen bonds between numerous hydroxyl groups in PVA and functional groups on the LMO surface result in a large amount of binder to be placed on the LMO surface as shown in Fig. 2. Note that the order in the Mn 2p peak intensity (PVA < PAN < PAA ≈ PVdF) is consistent with the order of the Mn dissolution in Table 1. This implies that higher binder coverage leads to lower Mn dissolution in LMO electrodes, confirming the role of the binder film as a passivation layer for Mn dissolution. This explains why PVA is so effective in suppressing the Mn dissolution despite its high HF content, and why PAA exhibits severe Mn dissolution in spite of its possible ionic interactions with Mn^{2+} ions. Although the roles of HF content and chemical interaction with Mn^{2+} ions cannot be totally ignored, all the evidences revealed so far equivocally support that Mn dissolution is mainly suppressed by binder layer on the LMO surface.

3.3. Adhesion strength and electrolyte uptake ratio

The adhesion strength of LMO electrodes and the electrolyte uptake ratio of binder films were compared (Table 2). PVA-LMO shows extremely high adhesion strength compared with the other electrodes, which is in line with its high surface coverage on the LMO surface (Fig. 2). The adhesion strength of PAN-LMO is similar to that of PVdF-LMO. The adhesion property of PAN is much lower than that of PVA, however their surface coverages are similar to each other. Since the adhesion is mainly determined by the interaction force between functional groups in the binder and aluminum current collector, this can be ascribed to much higher interaction of hydroxyl groups in PVA with the current collector compared with nitrile groups in PAN. PAA-LMO exhibits the lowest adhesion strength among the tested electrodes, which explains the low surface coverage of PAA as well as the low interaction of PAA with the current collector.

Besides the adhesion property, the electrolyte uptake behavior of the binder is an important factor for LIB performance. High electrolyte uptake by the binder promotes ion transport within the

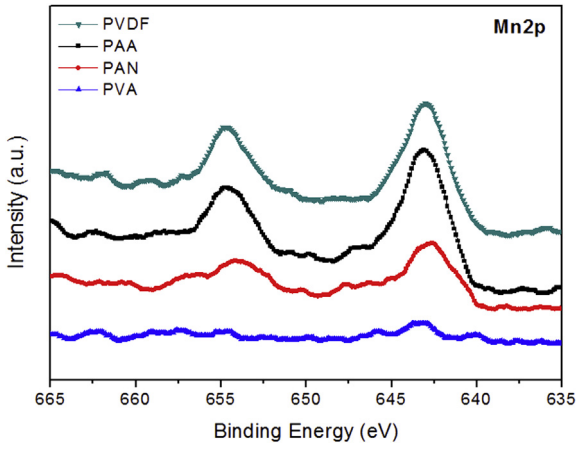

Fig. 2. Mn 2p XPS spectra for pristine LMO electrodes.

Table 2
Adhesion strength of LMO electrodes and electrolyte uptake ratio of binder films.

Binder	Adhesion strength (g_f cm^{-1})	Electrolyte uptake (%)
PAA	6.4	1.62
PAN	12.5	9.65
PVA	800.0	3.99
PVdF	14.0	19.29

composite electrode. In contrast, excess electrolyte uptake may weaken the adhesion capability of the binder, exacerbating problems with the mechanical integrity of electrodes [58,59]. Therefore, the optimum electrolyte uptake would secure both facile charge transport and mechanical stability, although the optimum value is still debatable. The electrolyte uptake ratio of a typical PVdF binder is known to be in the range of 20–30 wt.%, which is in good agreement with our result shown in Table 2. The order of the electrolyte uptake ratio is as follows: PVdF > PAN > PVA > PAA. This suggests that PVdF and PAN may show superior rate capability to PAA and PVA, which is examined in the next section.

3.4. Binder effects on LMO cell performances

In Fig. 3, the charge/discharge behaviors and rate capabilities of the LMO/Li cells are compared. It is clear that the binder greatly affects the electrochemical performances of LMO cells. PAA- and PVA-LMO cells show relatively short constant current charge and long constant voltage charge behaviors, and suffer from a large IR drop and activation overpotential compared with the PVdF-LMO cell (Fig. 3a). The PAN-LMO cell shows the smallest overpotential during the charge/discharge process among the tested cells. In addition, the 0.2C discharge capacity of the PAN cell (92.5 mAh g^{-1}) is higher than those of the other cells (91.3 mAh g^{-1} for PVdF, 81.7 mAh g^{-1} for PAA, and 69.7 mAh g^{-1} for PVA). Accordingly, the PAN-LMO cell exhibits superior rate capabilities compared to the others (Fig. 3b). The 2C discharge capacities (Q_{2C}) of the PAN-LMO cell are only 3.7 less than the 0.2C capacities ($Q_{0.2C}$), which indicates facile kinetics in the PAN-LMO cell. On the contrary, the PVdF-, PAA- and PVA-LMO cells show relatively large capacity drops in Q_{2C} (8.7%, 22.1%, and 52.8%, respectively). One of the reasons for the inferior kinetics of the PAA- and PVA-LMO can be legitimately ascribed to the relatively low electrolyte uptake of PAA and PVA binders (Table 2). In addition, excess coverage of the PVA binder on the active surface LMO, as demonstrated by XPS analysis (Fig. 2), seems to be partly responsible for the poor rate capability of PVA-LMO. The decreased discharge capacity and sluggish kinetics of PAA were also observed in a previous report, where the poor performances were ascribed to incomplete wetting with electrolyte [23]. The inferior discharge behavior of PAA-LMO was maintained even during the subsequent cycles (not shown here), which excluded the possibility of improper wetting problems in PAA-LMO.

The effects of binders on the cyclic performances were examined for LMO/graphite cells at both 25 °C and 60 °C (Fig. 4). Regardless of the temperature, the cyclability of the cells is in the following order: PAN > PAA > PVdF > PVA. Note that the PAN binder exhibits the highest cyclic capacity at the 300th cycle among the four different binders: 89.2 mAh g^{-1} at 25 °C and 37.2 mAh g^{-1} at 60 °C. The PAA-LMO electrodes exhibit slightly lower cyclic capacities (84.1 mAh g^{-1} at 25 °C and 30.0 mAh g^{-1} at 60 °C) than the PAN-LMO electrodes. It may be due to a relatively low HF concentration of the PAA-LMO when compared to the PVdF- and PVA-LMO electrodes (Table 1). Nevertheless, the PAA-LMO cells show much smaller initial capacities than the PAN-LMO cells, which is consistent with the previous results of initial capacity and rate capability

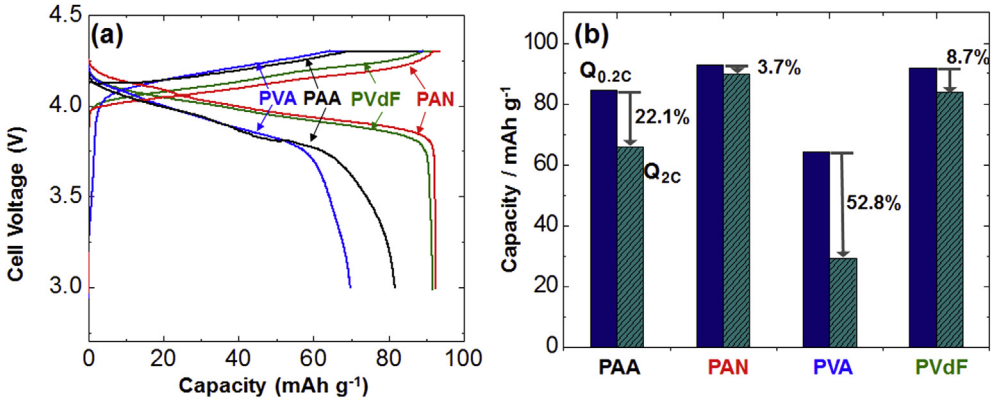

Fig. 3. (a) 0.2C charge and discharge profiles and (b) discharge capacities at 0.2C ($Q_{0.2C}$) and 2C (Q_{2C}) of LMO/Li cells. The ratio of reduced capacity (=($Q_{0.2C}$ − Q_{2C})/$Q_{0.2C}$*100) is also shown to represent rate capability in Fig. 3b.

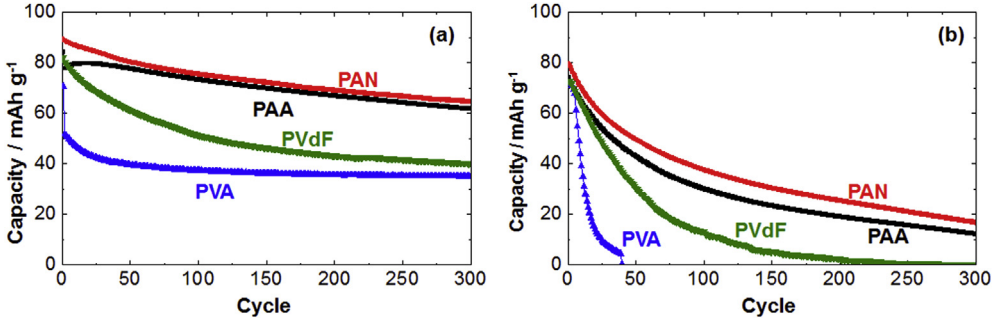

Fig. 4. Cyclic performances of LMO/graphite cells (a) at 25 °C and (b) at 60 °C.

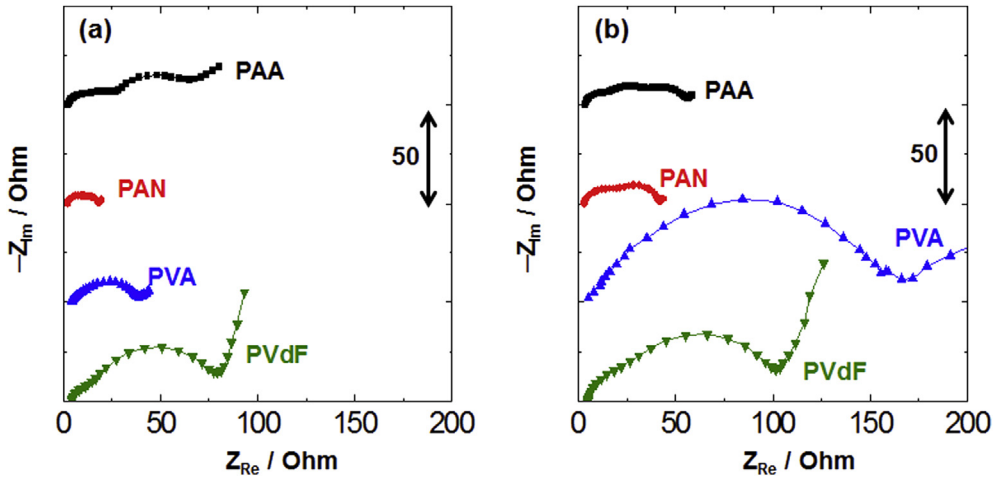

Fig. 5. Electrochemical impedance spectra of LMO/Li cells (a) before and (b) after 60 °C 24 h storage.

tests (Fig. 3). Again, the PVA-LMO exhibits the worst cycle performance. At 25 °C cycle, PVA shows quite low initial capacity but the cyclability is stabilized after 50th cycle, which can be explained by the excess coverage of PVA on the LMO surface acting as a resistive and protective layer. In our previous study [60], high surface coverage of the binder significantly decreased the electrochemical performance of $Li_4Ti_5O_{12}$ even though it improved the adhesion strength of the electrode. On the other hand, the kinetic hindrance imposed by excess binder coverage is supposed to be mitigated at 60 °C, and PVA exhibits high initial capacity comparable to the other binders. In this case, the high HF content generated from the PVA-LMO (Table 1) may be a main reason for its poor cyclability. In other words, even though the effective surface coverage by PVA suppresses the Mn dissolution of the LMO cathode, the high HF concentration seems to accelerate degradation of the graphite anode during cycle testing [9]. Indeed, it is noted that the cyclability order is in agreement with the order of HF concentration.

To better understand the role of the binder on the thermal stability of the LMO electrode, electrochemical impedance measurements were performed for LMO/Li cells before and after 60 °C 24 h storage (Fig. 5). Each impedance spectrum exhibits two semicircles in the high and middle frequency regions and an inclined line at the low frequency end. The impedance spectra are fitted with an equivalent circuit (Fig. 6), where R_s is the ohmic resistance, R_1 the resistance related to migration of the Li^+ ion through the surface film or due to the contact between the aluminum current collector and the active electrode composite [61,62], and R_2 the charge transfer resistance at the electrode/electrolyte interface. The capacitances associated with R_1 and R_2 are represented by the constant phase elements (CPEs), Q_1 and Q_2, respectively. The finite diffusion by a CPE, Q_D, is used to replace a Warberg element to fit the inclined line at the lowest frequency region [63,64]. The fitted values of R_1 and R_2 are compared in Fig. 7.

After storage at 60 °C, all the cells except the PAA-LMO show a considerable increase in the overall impedance, which is mainly driven by R_2. The order of R_2 after the 60 °C storage (PAN < PAA < PVdF < PVA) is the same as that of the 60 °C cycle performances (Fig. 4b). It is noted that the PAN-LMO exhibits the smallest values of R_1 and R_2 both before and after the 60 °C storage. PAN-LMO demonstrates excellent interfacial kinetics and thermal stability, which is consistent with its superior cell performances (Figs. 3 and 4). On the contrary, the PVA-LMO suffers from huge impedance build-up after storage, which is consistent with its poor cell performance. One possible explanation for the large impedance increase is that excess PVA coverage tends to detain dissolved Mn species, and thus facilitating the precipitation of resistive Mn compounds (Mn–F, Mn–O species) on the LMO surface [65]. The impedance of the PAA-LMO is slightly decreased after storage, a phenomenon for which a clear explanation is not available at the moment. It might be due to rearrangement of PAA binder in the composite electrode during storage. The reduced impedance of the PAA-LMO in storage may be related to its rather good cyclability at 60 °C (Fig. 4b).

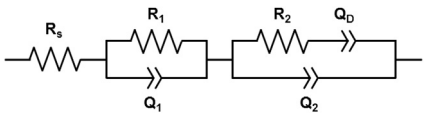

Fig. 6. Equivalent circuit for fitting of impedance spectra of LMO/Li cells in Fig. 5.

In brief, PAN is revealed to be an outstanding binder for LMO electrodes considering its excellent rate capability, superior cycle performance, and high thermal stability in comparison with the other three binders. In this study, the beneficial effects of PAN are highlighted only for LMO electrodes, but there will be every possibility that PAN can also improve other systems such as Ni-rich and high-voltage cathode materials, some of which are currently being investigated by our group. Since the molecular weight of polymer plays an important rule for the binder [30,52,58,60], further study on the effect of the molecular weight of PAN binder on the LMO electrode is also interesting.

4. Conclusions

The Mn dissolution of LMO electrodes is strongly dependent upon polymeric binders in the electrodes. The binder film on the surface of LMO plays a role in the passivation layer for Mn dissolution so that PVA and PAN binders covering the LMO surface suppress Mn dissolution, compared to PAA and PVdF binders. The PVA binder, however, suffers from low electrolyte uptake and excess surface coverage, leading to poor rate performance. Moreover, severe HF formation is probably associated with numerous hydroxyl groups in PVA, which results in inferior cyclability and large impedance increases at 60 °C storage. On the other hand, the PAN exhibits appropriate electrolyte uptake and extremely low impedance at both regardless of temperature. This contributes to the highest initial and cyclic capacities at 25 °C and 60 °C, which contributes to superior rate capability, cyclability and thermal

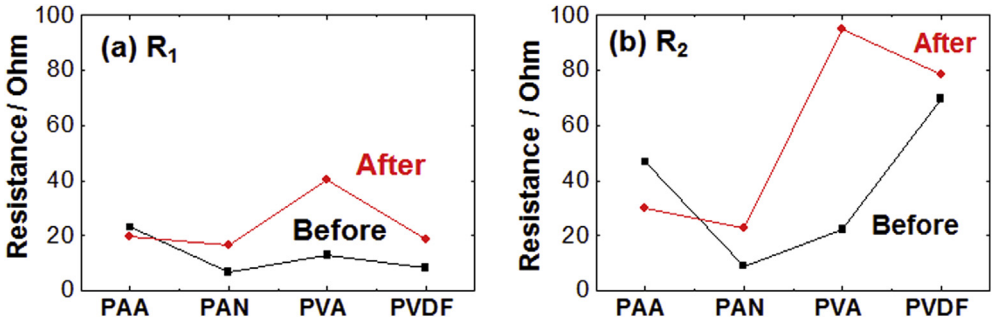

Fig. 7. Fitted values of R_1 and R_2 for LMO/Li cells.

stability of the LMO electrode containing the PAN binder. Consequently, the PAN is revealed to be an outstanding binder for LMO electrodes.

Acknowledgments

The work was supported by the Ministry of Science, ICT and Future Planning (NRF-2009-C1AAA001-2009-0093307). H. Lee is also grateful for financial support from the IT R&D program of MOTIE/KEIT (10041856, Technology development for life improvement of high Ni composition cathode at high temperature) and by the DGIST MIREBraiN program.

References

[1] M.S. Whittingham, Chem. Rev. 104 (2004) 4271–4302.
[2] Q. Zhong, A. Bonakdarpour, M. Zhang, Y. Gao, J.R. Dahn, J. Electrochem. Soc. 144 (1997) 205–213.
[3] J.C. Hunter, J. Solid State Chem. 39 (1981) 142–147.
[4] D.H. Jang, Y.J. Shin, S.M. Oh, J. Electrochem. Soc. 143 (1996) 2204–2211.
[5] Y. Xia, Y. Zhou, M. Yoshio, J. Electrochem. Soc. 144 (1997) 2593–2600.
[6] A. Blyr, C. Sigala, G. Amatucci, D. Guyomard, Y. Chabre, J.-M. Tarascon, J. Electrochem. Soc. 145 (1998) 194–209.
[7] A.D. Pasquier, A.B.P. Courjal, D. Larcher, G. Amatucci, B. Gerand, J.-M. Tarascon, J. Electrochem. Soc. 146 (1999) 428–436.
[8] R. Benedek, M.M. Thackeray, Electrochem. Solid-State Lett. 9 (2006) A265–A267.
[9] E. Wang, D. Ofer, W. Bowden, N. Iltchev, R. Moses, K. Brandt, J. Electrochem. Soc. 147 (2000) 4023–4028.
[10] H. Tsunekawa, S. Tanimoto, R. Marubayashi, M. Fujita, K. Kifune, M. Sano, J. Electrochem. Soc. 149 (2002) A1326–A1331.
[11] S. Komaba, N. Kumagai, Y. Kataoka, Electrochim. Acta. 47 (2002) 1229–1239.
[12] M. Ochida, Y. Domi, T. Doi, S. Tsubouchi, H. Nakagawa, T. Yamanaka, T. Abe, Z. Ogumi, J. Electrochem. Soc. 159 (2012) A961–A966.
[13] J.S. Kim, C. Johnson, J. Vaughey, S. Hackney, K. Walz, W. Zeltner, M. Anderson, M. Thackeray, J. Electrochem. Soc. 151 (2004) A1755–A1761.
[14] L. Xiong, Y. Xu, T. Tao, J.B. Goodenough, J. Power Sources 199 (2012) 214–219.
[15] J.-S. Kim, K. Kim, W. Cho, W.H. Shin, R. Kanno, J.W. Choi, Nano Lett. 12 (2012) 6358–6365.
[16] S. Komaba, B. Kaplan, T. Ohtsuka, Y. Kataoka, N. Kumagai, H. Groult, J. Power Sources 119 (2003) 378–382.
[17] S. Komaba, T. Itabashi, T. Ohtsuka, H. Groult, N. Kumagai, B. Kaplan, H. Yashiro, J. Electrochem. Soc. 152 (2005) A937–A946.
[18] M. Ochida, T. Doi, Y. Domi, S. Tsubouchi, H. Nakagawa, T. Yamanaka, T. Ab, Z. Ogumi, J. Electrochem. Soc. 160 (2013) A410–A413.
[19] Y. Liu, L. Tan, L. Li, J. Power Sources 221 (2013) 90–96.
[20] M.H. Fua, K.L. Huanga, S.Q. Liua, J.S. Liub, Y.K. Li, J. Power Sources 195 (2010) 862–866.
[21] M.-H. Ryou, G.B. Han, Y.M. Lee, J.N. Lee, D.J. Lee, Y.O. Yoon, J.K. Park, Electrochim. Acta 55 (2010) 2073–2077.
[22] M.-H. Ryou, S. Hong, M. Winter, H. Lee, J.W. Choi, J. Mater. Chem. A 1 (2013) 15224–15229.
[23] Z. Zhang, T. Zeng, Y. Lai, M. Jia, J. Li, J. Power Sources 247 (2014) 1–8.
[24] Z. Zhang, Z. Cao, T. Zeng, J. Li, M. Jia, J. Liu, Y. Lai, J. Electrochem. Soc. 160 (2013) A1353–A1357.
[25] M.E. Spahr, D. Goers, A. Leone, S. Stallone, E. Grivei, J. Power Sources 196 (2011) 3404–3413.
[26] N.S. Hochgatterer, M.R. Schweiger, S. Koller, P.R. Raimann, T. Wohrle, C. Wurm, M. Winter, Electrochem. Solid-State Lett. 11 (2008) A76–A80.
[27] G. Liu, S. Xun, N. Vukmirovic, X. Song, P. Olalde-Velasco, H. Zheng, V.S. Battaglia, L. Wang, W. Yang, Adv. Mater. 23 (2011) 4679–4683.
[28] I. Kovalenko, B. Zdyrko, A. Magasinski, B. Hertzberg, Z. Milicev, R. Burtovyy, I. Luzinov, G. Yushin, Science 334 (2011) 75–79.
[29] S. Komaba, K. Shimomura, N. Yabuuchi, T. Ozeki, H. Yui, K. Konno, J. Phys. Chem. C. 115 (2011) 13487–13495.
[30] H.-K. Park, B.-S. Kong, E.-S. Oh, Electrochem. Commun. 13 (2011) 1051–1053.
[31] L. Gong, M.H.T. Nguyen, E.-S. Oh, Electrochem. Commun. 29 (2013) 45–47.
[32] H. Buqa, M. Holzapfel, F. Krumeich, C. Veit, P. Novák, J. Power Sources 161 (2006) 617.
[33] Z. Chen, L. Christensen, J.R. Dahn, Electrochem. Commun. 5 (2003) 919.
[34] Z. Chen, L. Christensen, J.R. Dahn, J. Appl. Polym. Sci. 91 (2004) 2958.
[35] J.H. Lee, U. Paik, V.A. Hackley, Y.M. Choi, J. Electrochem. Soc. 152 (2005) A1763.
[36] F.M. Courtel, S. Niketic, D. Duguay, Y. Abu-Lebdeh, I.J. Davidson, J. Power Sources 196 (2011) 2128.
[37] A. Magasinski, B. Zdyrko, I. Kovalenko, B. Hertzberg, R. Burtovyy, C.F. Huebner, T.F. Fuller, I. Luzinov, G. Yushin, ACS Appl. Mater. Interfaces 2 (2010) 3004–3010.
[38] J.S. Kim, W. Choi, K.Y. Cho, D. Byun, J. Lim, J.K. Lee, J. Power Sources 244 (2013) 521–526.
[39] Z. Zhang, W. Bao, H. Lu, M. Jia, K. Xie, Y. Lai, J. Li, ECS Electrochem. Lett. 1 (2012) A34–A37.
[40] Z. Zhang, T. Zeng, H. Lu, M. Jia, J. Li, Y. Lai, ECS Electrochem. Lett. 1 (2012) A74–A76.
[41] S. Komaba, N. Yabuuchi, T. Ozeki, Z. Han, K. Shimomura, H. Yui, Y. Katayama, T. Miura, J. Phys. Chem. C. 116 (2012) 1380–1389.
[42] Y.-S. Park, E.-S. Oh, S.-M. Lee, J. Power Sources 248 (2014) 1191–1196.
[43] Z. Wang, N. Dupre, A.-C. Gaillot, B. Lestriez, J.-F. Martin, L. Daniel, S. Patoux, D. Guyomard, Electrochim. Acta 62 (2012) 77–83.
[44] J. Li, R. Klöpsch, S. Nowak, M. Kunze, M. Winter, S. Passerini, J. Power Sources 196 (2011) 7687–7691.
[45] Z.H. Ping, Q.T. Nguyen, S.M. Chen, J.Q. Zhou, Y.D. Ding, Polymer 42 (2001) 8461–8467.
[46] S.E. Sloop, J.K. Pugh, S. Wang, J.B. Kerr, K. Kinoshita, Electrochem. Solid-State Lett. 4 (2001) A42–A44.
[47] C.G. Barlow, Electrochem. Solid-State Lett. 2 (1999) 362–364.
[48] U. Heider, R. Oesten, M. Jungnitz, J. Power Sources 81-82 (1999) 119–122.
[49] T. Gotoh, K. Matsushima, K.I. Kikuchi, Chemosphere 55 (2004) 57.
[50] B. Conti, B. Colzani, A. Papetti, D. Mascherpa, R. Dorati, I. Genta, C. Pruzzo, C. Signoretto, E. Zaura, P. Lingström, Food Chem. 138 (2013) 898.
[51] C. Gok, S. Aytas, J. Hazard. Mater. 168 (2009) 369.
[52] M. Yoo, C.W. Frank, S. Mori, Chem. Mater. 15 (2003) 850–861.
[53] C.-Y. Chiang, Y.J. Shen, M.J. Reddy, P.P. Chu, J. Power Sources 123 (2003) 222–229.
[54] M. Park, X. Zhang, M. Chung, G.B. Less, A.M. Sastry, J. Power Sources 195 (2010) 7904–7929.
[55] R.J. Brodd, W. Huang, J.R. Akridge, Macromole. Sym 159 (2000) 229–245.
[56] K. Xu, Chem. Rev. 104 (2004) 4303–4417.
[57] M. Ue, S. Mori, J. Electrochem. Soc. 142 (1995) 2577–2581.
[58] M. Yoo, C.W. Frank, S. Mori, S. Yamaguchi, Polymer 44 (2003) 4197–4204.
[59] L. Chen, X. Xie, J. Xie, K. Wang, J. Yang, J. Appl. Electrochem 36 (2006) 1099–1104.
[60] B.-R. Lee, E.-S. Oh, J. Phys. Chem. C. 117 (2013) 4404–4409.
[61] J.-M. Atebamba, J. Moskon, S. Pejovnik, M. Gaberscek, J. Electrochem. Soc. 157 (2010) A1218–A1228.
[62] J. Illig, M. Ender, T. Chrobak, J.P. Schmidt, D. Klotz, E. Ivers-Tiffee, J. Electrochem. Soc. 157 (2012) A952–A960.
[63] Q.-C. Zhuang, T. Wei, L.-L. Du, Y.-L. Cui, L. Fang, S.-G. Sun, J. Phys. Chem. C. 114 (2010) 8614–8621.
[64] X.-Y. Qiu, Q.-C. Zhuang, Q.-Q. Zhuang, R. Cao, P.-Z. Ying, Y.-H. Qiang, S.-G. Sun, Phys. Chem. Chem. Phys. 14 (2012) 2617–2630.
[65] D. Kim, S. Park, O.B. Chae, J. Ryu, Y.-U. Kim, R.-Z. Yin, S.M. Oh, J. Electrochem. Soc. 159 (2012) A193–A197.